Impact of two radio occultation constellations on numerical weather prediction: polar-orbits only and mixed polar-equatorial orbits

Nikki C. Privé[1], Christopher Barsoum[2,3], Douglas Hunt[4], Michael J. Murphy[5], Richard Anthes[4], William Gullotta[4], Natalie Laudier[2]

[1]Goddard Earth Sciences Technology and Research II, Morgan State University, Baltimore, MD, USA
[2]National Environmental Satellite, Data, and Information Service, NOAA, Silver Spring, MD, USA
[3]The Aerospace Corporation, USA
[4]University Corporation for Atmospheric Research, Boulder, CO, USA
[5]Goddard Earth Sciences Technology and Research II, University of Maryland Baltimore County, Baltimore, MD, USA

Key Points:

- A constellation with a mix of polar- and Equatorial orbiting satellites produces better forecasts than a constellation of all polar orbits.
- All local time coverage and a higher tropical observation density are associated with the mixed polar-equatorial constellation.
- GNSS-RO observation information is generally well-retained by the forecast model for 6-12 hours.

Corresponding author: Nikki C. Privé, `nprive@alum.mit.edu`

Abstract

This study explores the relative impact of two orbital configurations for Global Navigation Satellite System radio occultation (RO) observations in numerical weather prediction (NWP) using observing system simulation experiments (OSSE). Three experiments are carried out: a Control experiment with no RO observations and two experiments with 14,000 RO profiles per day - one with only polar orbiting satellites which provides a high concentration of profiles in the extratropics but has gaps in spatial coverage every six hours, and a second with a mix of polar and equatorial orbits with RO profiles that are more concentrated in the tropics and has a more uniform local time coverage. Both experiments with RO included show an increase in forecast accuracy compared to the Control. The mixed orbit case shows a significant improvement in forecast accuracy compared to the polar-only orbit case in the tropics.

The OSSE framework allows calculation of observation impacts on background and analysis errors, so that the contribution of information from retained RO information can be compared with the contribution of new information from observations ingested in the current cycle. Impacts of RO in the two sampling experiments are also explored using a forecast sensitivity observation impact tool for 24-hour forecasts, and by comparing the skill of medium-range forecasts. In stratospheric midlatitudes, the RO observational information is well retained, so that more frequent sampling is not required. However, the Tropics are found to be particularly sensitive to RO data in both the stratosphere and troposphere, and relatively uniform coverage is advantageous.

1 Introduction

Over the past two decades Global Navigation Satellite System radio occultation (GNSS-RO) data has been an important component of the global observing network for numerical weather prediction (NWP). Bending angles derived from GNSS-RO provide sounding-type information about temperature and humidity primarily in the stratosphere and mid- to upper troposphere, with ongoing efforts to improve the use of RO data in the lower troposphere. RO observations have been shown in numerous studies to provide significant improvement to operational weather forecasts (Healy & Thépaut, 2006; Aparicio & Deblonde, 2008; Cucurull & Derber, 2008; Rennie, 2010). Recent efforts to determine observational requirements for future planning of the global observing network (NOAA SPRWG, 2018; Anthes et al., 2019) ranked RO as a high priority, recommending the expansion of RO to at least 20,000 soundings per day (Anthes et al., 2024). This recommendation was based largely on numerous recommendations from the International Radio Occultation Working Group (IROWG).

RO data have been provided for operational use by multiple government-sponsored platforms including both polar (e.g., the European Organisation for the Exploitation of Meteorological Satellites (EUMETSAT)'s Meteorological Operational satellites program (MetOp) satellites (von Engeln et al., 2009)) and inclined/equatorial orbital systems such as the Formosa Satellite Mission-7 (FORMOSAT-7)/Constellation Observing System for Meteorology, Ionosphere, and Climate-2 (hereafter COSMIC-2) mission (Anthes & Schreiner, 2019; Schreiner et al., 2020; Ho et al., 2020). While commercial RO data have become more prolific in recent years, the spatiotemporal variability of commercial datasets may vary over time depending on launch availability and other factors. Given the uncertainty in the spatiotemporal distribution of commercial RO data, there has been interest in a possible government-run network of GNSS platforms that would provide baseline coverage of the globe (Gail et al., 2025). Because the largest government-run RO mission, COSMIC-2, which is in a low-inclination orbit and provides over 5,000 profiles per day in the tropics and subtropics, is approaching the end of its expected lifespan, the National Environmental Satellite, Data, and Information Service (NESDIS) has conducted a radio occultation Analysis of Alternatives (AoA) study to evaluate future needs for a global network of RO platforms.

One question explored by the AoA was the importance of a constellation in low-inclination (Equatorial) orbits similar to COSMIC-2 in addition to a constellation of high-inclination (polar) orbits. This paper studies this question by comparing the impact on NWP of two realistic constellations with the same number (14,000) of RO profiles a day globally, a polar-only constellation and a mixed polar-equatorial constellation. The mixed constellation provides denser observations in the tropics and uniform local time coverage, while the polar constellation provides denser observations in middle and high latitudes, but has gaps in the local time coverage. The IROWG has recommended all local time coverage for future constellations (Anthes et al., 2024), largely because of climate and space weather applications. Although there are recommendations for 20K global profiles per day, the 14K number in this study was chosen because it represented the number of RO observations available from both government and commercial missions at the time of the start of this study (2023). Another AoA study investigated the impact of 20K profiles per day (Cucurull et al., 2026).

There are numerous studies documenting the importance of uniform temporal coverage for climate monitoring (for example, Leroy, 2001; Kirk-Davidoff et al., 2005) because diurnal variations of temperature in the lower troposphere and stratosphere (where there is ozone heating) can create temporal biases in climate data records that obscure trends. All local time coverage is essential for space weather monitoring, because solar effects on the ionosphere and magnetosphere vary strongly between night and day. However, the importance of uniform temporal coverage on NWP is less obvious, and there are no studies that we know of on the sensitivity of NWP analyses and forecasts to temporal sampling. Several studies, however, have suggested that uniform time sampling is preferable to sampling only at certain local times. In a study of orbital effects of three microwave sounders, di Tomaso and Bormann (2011) showed that three sounders in three different orbits (with different equatorial crossing times) showed greater forecast impact than three satellites with only two equatorial crossing times. Eyre and Weston (2014) indicated that polar orbiting satellites should be equally spaced in time and that the degree of improvement depends on the growth rate of the forecast errors. The importance of uniform local time coverage was found to be much more important when the growth of errors was fast, as expected in cases of high-impact weather events such as rapidly developing extratropical or tropical cyclones. They concluded that satellites should be deployed in orbits that are approximately equally spaced where possible.

At the heart of the temporal coverage requirement is the retention of information from RO in the NWP system. If the information content from RO is well-retained, a long refresh interval with more sparse observations could be acceptable. However if the information content from RO is rapidly lost, a more frequent refresh rate and more dense observations would be more effective. One factor that affects the retention of observation information in the forecast is the rate and magnitude of model error growth, as implied by Eyre and Weston (2014). Rapid error growth, as occurs in strong baroclinic zones or in regions of tropical cyclone genesis, will tend to destroy retained information content, whereas regions with slow error growth are more likely to retain information. Fast model error growth is generally associated with the handling of physical atmospheric processes in the model, such as moist convection and boundary layer dynamics, as well as regions of atmospheric instability, especially near the jet stream. The inherent timescale for initial value error growth due to atmospheric dynamics can also play a role, with an expectation that error growth saturates first at the smallest spatial scales, cascading over time to the planetary scale as the forecast extends into the long term (Lorenz, 1969).

Another factor that affects the retention of observation information is the ability of the data assimilation system (DAS) to ingest the information such that the analysis state is properly balanced. If the initial state is not suitably balanced, geostrophic adjustment will occur to bring the atmosphere into a balanced state (Morel & Talagrand, 1974; Vallis, 1991), potentially losing information content in the process. In the extra-tropics, geostrophic balance can be used to infer wind information from mass information, so that temperature observations are highly useful for constraining the state of the atmosphere (Charney et al., 1969; Smagorinsky et al., 1970). However, in the Tropics where geostrophic balance is weak or not applicable, temperature observations have been found to be less useful than wind observations for initializing the atmospheric state (Li et al., 2023), and more frequent temperature observations are required.

Observing system simulation experiments (OSSEs) can be used to study different spatiotemporal configurations of observations in a sophisticated and realistic NWP framework (Atlas & Emmitt, 2008; Atlas & Riishojgaard, 2008; Hoffman & Atlas, 2016; Boukabara et al., 2018; R. M. Errico & Privé, 2018). In an OSSE, all elements of the global observing network are simulated, including the atmosphere, which is modeled by a simulated Nature Run. The availability of the Nature Run allows the direct calculation of the analysis and background error fields, and thus the observation impact on the analysis and background fields can be derived by performing a series of experiments with and without a particular subset of observations. Different observing experiments can be simulated and compared in the OSSE without the need for real observations. Different GNSS-RO configurations have been the subject of multiple OSSEs (Cucurull et al., 2018; Cucurull & Mueller, 2020; Privé et al., 2022), and have shown that additional RO observations generally improve the short and medium-range forecast. However these studies did not focus on the impact of the temporal frequency of RO observations.

Observation impacts on NWP are affected by the information content of the observations, the error growth characteristics during the forecast, the availability of other observing types, and the retention of observation information. Observations may contain information that is largely redundant with other contemporaneous observations, or with information retained from observations at previous cycle times. In an OSSE framework, comparison of the impact of observations on the background state and on the analysis state can be used to evaluate some aspects of redundancy of the observation information with retained information from previous cycles. The length of forecast lead time at which the observations maintain significant impact is an indicator of the ability of the NWP framework to retain observation information. Prior studies have found that the largest observation impacts generally occur at the initial time, with longer retention of RO observation impacts in the midlatitudes compared to the Tropics (Privé et al., 2022).

The goal of these experiments is not to find the optimal orbital configuration for a fixed number of profiles per day, which would require numerous OSSEs, but instead to compare the impact on NWP of two possible orbital scenarios representing different extremes of spatio-temporal observation distributions. Observations simulated for actual orbital calculations were used rather than artificially distributing RO observations without considering orbital realism.

The National Aeronautics and Space Administration Global Modeling and Assimilation Office (NASA/GMAO) OSSE framework is used to conduct the observation impact studies. This framework has been extensively calibrated and validated to ensure that the behaviors of the simulated system are representative of the real world (R. M. Errico et al., 2013; Privé et al., 2023). One of the advantages of this framework is the availability of the Forecast Sensitivity Observation Impact (FSOI) tool that uses a linearized version of the forecast model to estimate the relative impact of all ingested data types on the short term forecast skill. Numerous observation impact studies have been carried out using the GMAO OSSE framework, including for microwave radiances, geostationary hyperspectral infrared radiances, atmospheric motion vectors, and spaceborne radar for measuring marine surface pressures (McCarty et al., 2021; McGrath-Spangler et al., 2022; Privé, McLinden, et al., 2024; Privé, McGrath-Spangler, et al., 2024). This work will closely follow the methodology used for prior RO OSSE studies of potential saturation of RO information when large quantities of RO data are ingested (Privé et al., 2022).

The manuscript is organized as follows: the OSSE framework, simulation of RO observations, and experiment setup are described in Section 2. Section 3 compares the impacts of RO observations on the analysis state in the two experiments, and Section 4 describes the RO impacts on the short to medium range forecast skill. The estimates of observation impact on short-range (24-h) forecasts calculated with the FSOI tool are shown in Section 5, and a summary and discussion of the overall results are given in Section 6.

2 Method

The framework used for these experiments is an updated version of that employed for previous RO studies with the GMAO OSSE (Privé et al., 2022). The upgrades to the framework are described in detail by Privé et al. (2023), with a basic overview given in the following section. The simulation of RO bending angles is similar to that of the previous OSSE studies, with the main difference being a more sophisticated method of simulating the orbits and spatiotemporal locations of the RO soundings.

2.1 OSSE Overview

The GMAO OSSE framework consists of a Nature Run (NR), simulated observations for most of the data types used for operational numerical weather prediction, and a data assimilation system and forecast model used to produce the experiment analyses and forecasts. The NR is a long free forecast of a high resolution global model that simulates the real atmosphere. The NR fields are used for generating the simulated observations, and also for verification and validation of the analysis and forecast errors. In this version of the GMAO OSSE framework, the Global Earth Observing System version 5 (GEOS-5) model was used to produce a two year NR with 7 km horizontal resolution, 72 vertical levels, and 30 minute output. This NR is commonly referred to as the G5NR, and it has been extensively validated (Gelaro et al., 2014).

Simulated observations are generated by interpolating the NR fields to the spatiotemporal locations of real observations from a selected time period, along with the potential use of an observation operator depending on the observation type. In situ data types such as rawinsondes, surface observations, and aircraft are simply interpolated. Radiance observations use interpolated profiles from NR fields along with the Community Radiative Transfer Model (CRTM, Han et al. (2006)) to simulate brightness temperatures. Contamination of infrared radiances by clouds is determined using the NR cloud fields, and contamination of microwave radiances by precipitation is similarly dependent on the NR precipitation fields. Infrared radiance data types include the Atmospheric Infrared Sounder (AIRS), Infrared Atmospheric Sounding Interferometer (IASI), and Cross-track Infrared Sounder full spectral resolution (CrIS-FSR), and microwave radiance types include Advanced Microwave Sounding Unit (AMSU-A) and Advanced Technology Microwave Sounder (ATMS). The Microwave Humidity Sounder (MHS), Advanced Microwave Scanning Radiometer 2 (AMSR-2), Special Sensor Microwave Imager / Sounder (SSMIS), and Global Precipitation Measurement (GPM) Microwave Imager (GMI) are simulated and assimilated using all sky assumptions. Locations of atmospheric motion vectors (AMVs) are based on the cloud and moisture fields of the NR along with the footprints of geostationary and MODIS satellites. A full description of the simulation methods is given in R. Errico et al. (2017) and Privé et al. (2023).

Since the magnitude and characteristics of observation errors are crucial to the handling of the observations by the DAS and thus to the observation impacts, simulated observation errors are added to the simulated observation data. The magnitude of the simulated errors is adjusted so that the standard deviation of observation innovation (observation minus background, O-B) for each simulated data type matches that of real observations. While purely uncorrelated simulated errors are added to some data types, such as surface observations and aircraft, other data types receive a mix of uncorrelated and correlated random errors. Rawinsondes and AMVs have vertically correlated error, hyperspectral infrared radiances have channel-correlated errors, and other radiances along with AMVs have horizontally correlated errors. The correlation characteristics are selected to match the correlation of real observations.

The data assimilation system and forecast model are selected to be the same version that was quasi-operational at the GMAO in early 2023. The GEOS model (Rienecker et al., 2008) at 25 km horizontal resolution with 72 vertical levels is used for the forecast model. The data assimilation system is the 4-dimensional hybrid ensemble variational (Hybrid 4D-EnVar) Gridpoint Statistical Interpolation (GSI). Privé et al. (2023) describe and illustrate the performance of the GMAO OSSE framework with this configuration.

The assumed uncertainty model applied to the simulated bending angles during ingestion by the DAS is an important part of the data assimilation system used to produce the analyses and forecasts in the experiments. The uncertainty model employed for this study is the same as that used operationally at the ECMWF and was described in Ruston and Healy (2021). The observations of bending angle at each tangent point over the globe are all given the same treatment in this model, which only varies the uncertainties as a function of impact height (a geometric coordinate used in GNSS-RO that takes into account the refractive index of the Earth's atmosphere) in the vertical. Uncertainties are assigned a value of 20% of the observed bending angle value at 0 km impact height, decreasing linearly with impact height to 1.25% at 10 km. A constant uncertainty of 1.25% is used above 10 km until the lower limit of the uncertainty model is reached, which is 3 microradians. The uncertainty model is shown in Figure 1.

2.2 Simulation of RO Data

Simulation of the RO data was undertaken in three steps. First, the spatiotemporal locations of each tangent point (point closest to the surface of the Earth along each RO ray path) in the RO soundings was calculated using orbital simulation to determine when and where pairs of orbiting platforms would be in conjunction so as to allow atmospheric sampling. Next, these locations were used along with the NR fields to generate bending angles at each tangent point using the 2-dimensional forward model included in the Radio Occultation Processing Package (ROPP2D, ROM SAF, 2021). Finally, simulated observation errors were added to the simulated bending angles so that the simulated RO data would have similar characteristics to those of real RO data.

The spatiotemporal locations of the RO profiles were calculated using idealized Keplerian propagation of a series of satellites. Satellite rise-set times were computed between the observing satellites and all four major GNSS constellations (GPS, GLONASS, Galileo, BeiDou) using a limb-facing sensor field of view pointing at the horizon with an elevation angle sufficient to achieve a maximum occultation point geodetic altitude of 150 km. One sensor was mounted on the forward plane of the satellite in the in-track direction, while another was mounted on the aft plane in the in-track direction. The occultation point's Euclidean position in an Earth-centered inertial frame was recorded at a sampling rate of 50 Hz at rise time minus 100 seconds all the way through set time plus 100 seconds.

The ROPP2D forward model is based on the two-dimensional bending angle operator employed at the European Centre for Medium-Range Weather Forecasts (ECMWF, Healy et al., 2007) in their Integrated Forecast System (IFS, e.g., Ruston & Healy, 2021). For this study it was configured to enable the 2-dimensional ray tracing capability only

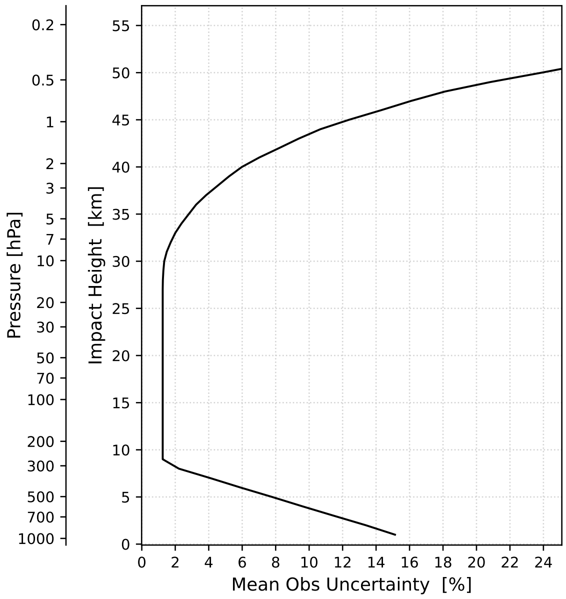

Figure 1. Mean error (%) assigned to all simulated GNSS-RO observations over the globe in the RO data assimilation experiments. These uncertainties are assigned within the DA system based on the impact height of the given observation, a geometric coordinate used in GNSS-RO that takes into account the refractive index of the Earth's atmosphere. Vertical bins with width of 1 km impact height are used for the statistics and the approximate corresponding atmospheric pressure is shown in a secondary vertical axis for reference.

below 10 km atmospheric height. The G5NR temperatures used with ROPP2D in the stratosphere are smoothed with a simple filter to remove an erroneous 'stair-step' feature introduced by a problem with temperature remapping during the generation of the NR fields. This smoothing is described in detail in Privé et al. (2022) and was not required in the troposphere. While the ROPP2D operator is used to simulate the bending angles, the one-dimensional NCEP Bending Angle Method (NBAM, Cucurull et al., 2013) operator is used by the GSI to ingest the data. It is preferred to use a different operator for simulation and assimilation of synthetic data to introduce operator error into the simulated observations and thus mitigate the twinning issue in OSSEs.

Observation errors stem from multiple sources, as summarized by Anthes et al. (2022). In the GMAO OSSE framework, there is some degree of operator error due to the use of different operators to simulate and to assimilate the RO. However, instrument and representativeness errors are generally lacking compared to real observations. The simulated RO errors are calibrated by simulating the 2020-based RO data and comparing the statistics of observation innovation for the simulated RO data with the observation innovations for real RO ingested for the same time period. The 2020 GNSS-RO data used to calibrate the simulated RO errors included Metop-A, -B, -C, TerraSAR-X, TanDEM-X, PAZ, COSMIC-2, and KOMPSAT-5, which were treated in bulk for calculations of observation innovations. The simulated errors include a random uncorrelated component as well as a vertically correlated random component, selected to match the vertical correlation of real RO data with a Gaussian distribution and characteristic length scale of 300 m.

The magnitude of the simulated errors varies with both latitude and height as described in detail in Privé et al. (2022), because errors particularly in the troposphere are

Table 1. Simulated observing platforms for GNSS-RO. SSO refers to Sun Synchronous Orbits.

Orbit Type	Platforms	Control	Polar	Mix
Equatorial Walker	6			X
Polar Walker	6			X
Higher Altitude SSO	2		X	
Lower Altitude SSO	9		X	

affected by the presence of moisture. GNSS-RO O-F variance is highest within 20° of the equator, and with somewhat higher variances in the northern hemisphere. The latitudinal dependence of the observation errors is most pronounced in the troposphere, with weaker dependence in the stratosphere. Latitude bins of 5° width were used to calculate the target statistics for the simulated RO errors.

2.3 Experiment Setup

A Control and two experiments were run from 1 July to 30 September in the second year of the NR. For the Control case, the simulated global observing network is based on the 2020 observing network but with all RO data excluded. Calibration and spinup of the OSSE is performed during the month of June in the second year of the G5NR. The iterative nature of the calibration process allows the satellite bias coefficients to spin up over what is effectively a much longer period, in this case on the order of several months. The experiment period is from 1 June to 30 September in the second year of the G5NR. Analyses are produced four times daily, at 0000, 0600, 1200, and 1800 UTC. Short 24-h forecasts are initialized from the analyses four times daily, along with the use of the FSOI tool. Longer seven day forecasts are initialized once daily starting from the 0000 UTC analysis.

The Polar experiment adds RO observations from a set of eleven polar orbiting platforms, as indicated in Table 1. For the Polar experiment, eleven satellites using a 90 degree field of view for both forward and aft antennas were used to represent a "worst possible" realistic case of satellite spatial-temporal distribution. These orbits were selected semi-randomly from a pool of known current or future RO missions in sun synchronous orbits (SSO) constrained to equatorial crossing times in the morning only (0900 - 1100 local time). Their orbit altitude parameters were modified slightly to ensure the set of satellites did not feature any discernible resonances or synchronicities with one another, so as to simulate a lack of consideration for spatial-temporal distribution. A small portion of RO observations from both experiment cases were randomly removed to bring the daily average of observations as close to 14,000 as possible, with roughly 3,500 soundings for each cycle time.

The average count of RO observations (not soundings) per 500 km by 500 km areal bins is shown in the top panels of Figure 2 for the Polar experiment over all cycle times and also for the distribution corresponding to the 0000 UTC and 1800 UTC cycle times. The greatest density of RO observations in the Polar experiment is over the polar regions with a minimum over the Tropics. For individual cycle times, there is an orbital swath under which the observational density is high, with gaps in which there are no RO observations. While there are some regions that have some orbital coverage more frequently than every twelve hours, most areas are observed twice daily at twelve hour intervals and there are gaps every six hours that move westward during the day.

For the experiment with a mix of equatorial and polar orbits, twelve satellites using a 120 degree field of view for both forward and aft antennas were used to represent

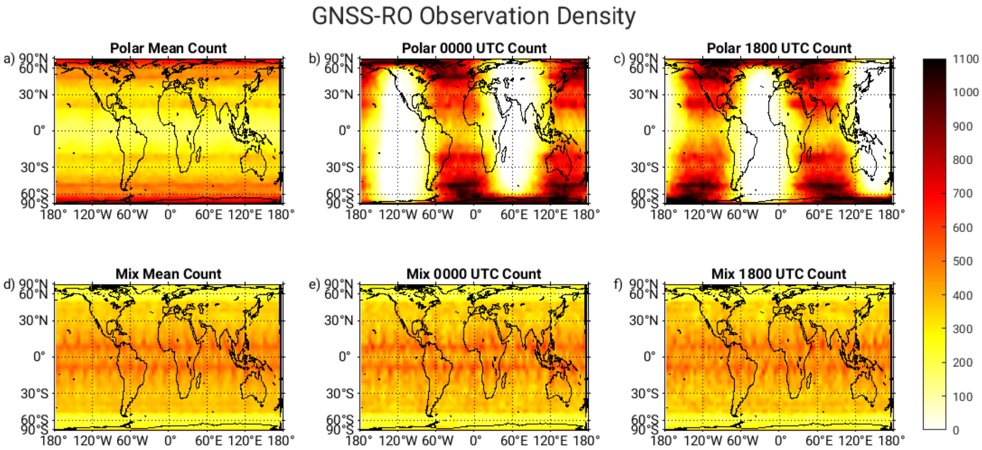

Figure 2. Heat maps of observation density (numbers per approximately 500km by 500km areal bins), averaged over three months. Left panels, daily mean observation density per cycle time; center panels, observation density for the 0000 UTC analysis cycle; right panels, observation density for the 1800 UTC analysis cycle. Top row, Polar experiment; bottom row, Mix experiment.

a roughly “best possible” case of satellite spatiotemporal distribution. These orbits were selected in a two-segment constellation for optimal 6-hour global refresh as shown in Table 1. The orbits include a 30-degree inclined low-inclination Walker constellation and a 90-degree inclined high-inclination Walker constellation. An additional satellite was necessary in the Mix experiment to ensure that the counts between the two experiments remained the same. Heat maps of RO observation density for the Mix experiment are shown in the bottom panels of Figure 2. The greatest density of RO observations in the Mix experiment is in the Tropics, with similar distributions at all four cycle times. As with the Polar experiment, there are approximately 14,000 RO soundings per day in the Mix experiment.

In standard operational cycling mode, the NWP process uses a background field taken from a previous forecast - in this case six hours prior - and performs data assimilation to produce a new analysis, and then initiates a new forecast based on the new analysis. This forecast then provides the background for the next analysis cycle. In cycling mode, the information content from the ingested observations accumulates in the background in addition to the information stemming from the current cycle batch of observational data.

An alternative method of producing analyses can be performed in which RO observation information from the current cycle time is isolated. In this method, referred to as ‘Standalone’, the backgrounds are taken from the Control run and the forecast model is not integrated between cycle times. Only the DAS is run for each cycle time, ingesting both the global observations from the Control case as well as the RO data. As a result, the Standalone analyses contain only the RO information ingested during the current cycle, while simultaneously carrying forward information for all other previously ingested observation types. Every analysis cycle is carried out as if it were the first cycle for which RO data were assimilated. This is illustrated in (1) and (2) for the cycling method and (3) for Standalone below:

$$\mathbf{x_a^{ctl}} = \mathbf{x_b^{ctl}} + \mathbf{K}(\mathbf{y^{ctl}} - \mathbf{H^{ctl}}\mathbf{x_b^{ctl}}) \quad (1)$$

$$\mathbf{x_a^{exp}} = \mathbf{x_b^{exp}} + \mathbf{K}(\mathbf{y^{exp}} - \mathbf{H^{exp}}\mathbf{x_b^{exp}}) \quad (2)$$

$$\begin{aligned} \mathbf{x_{sa}^{exp}} &= \mathbf{x_b^{ctl}} + \mathbf{K}(\mathbf{y^{exp}} - \mathbf{H^{exp}}\mathbf{x_b^{ctl}}) \\ &= \mathbf{x_b^{ctl}} + \mathbf{K}(\mathbf{y^{ctl}} - \mathbf{H^{ctl}}\mathbf{x_b^{ctl}}) + \mathbf{K}(\mathbf{y^{RO}} - \mathbf{H^{RO}}\mathbf{x_b^{ctl}}) \\ &= \mathbf{x_a^{ctl}} + \mathbf{K}(\mathbf{y^{RO}} - \mathbf{H^{RO}}\mathbf{x_b^{ctl}}), \end{aligned} \quad (3)$$

where $\mathbf{H}$ is the observation operator, $\mathbf{K}$ is the Kalman gain, $\mathbf{x_a}$ is the analysis state, $\mathbf{x_{sa}}$ is the Standalone analysis state and $\mathbf{x_b}$ is the background state for the Control (ctl) and experiment (exp) cases, and RO indicates the set of all GNSS-RO observations.

Comparison of the Standalone analyses with the Control analyses isolates the impact of the RO observations on the current analysis while excluding both accumulation of RO information and complications due to model feedbacks and differing backgrounds. Standalone mode is commonly used in practice for testing data assimilation and observing system changes. The observation impact is the difference between the Control and experiment analyses. Both cycling and Standalone experiments were run for the Mix and Polar experiments and these results will be compared.

3 Analysis Impacts

Analysis errors can be directly calculated for model fields by verifying the analysis state against the NR fields regridded to the same resolution. The root-temporal-mean-square error (RMSE) at each model gridpoint is calculated for the Control and each of the experiment runs using four times daily analysis states from July to September. The observation impact of RO data on the analysis state ($\Delta RMSE$) is calculated and normalized ($RMSE_N$) by the Control RMSE as follows:

$$\Delta RMSE = RMSE_{Exp} - RMSE_{Control} \quad (4)$$

$$RMSE_N = \frac{\Delta RMSE}{RMSE_{Control}} \quad (5)$$

For these calculations, negative $\Delta RMSE$ and $RMSE_N$ indicate an improvement, or reduction in the analysis error, when RO data are included. A value of -0.1 for $RMSE_N$ can be interpreted as a 10% reduction in RMSE of the experiment case analysis error compared to Control.

3.1 Daily Impacts

First, results are shown considering all four analysis cycle times per day in the calculations of $RMSE_N$ to evaluate the overall impacts of RO in the two experiments. The zonal mean $RMSE_N$ for temperature, specific humidity, and zonal wind analyses are shown in Figure 3 for the Polar experiment, Mix experiment, and difference between Mix and Polar experiments. For the left and center columns, blue coloration indicates that both RO experiments have a beneficial impact on the analysis state compared to Control, in agreement with many previous OSE and OSSE studies. In the right column, blue coloration indicates that the Mix experiment has a more beneficial RO impact than the Polar experiment.

Overall, the impacts of RO in the Polar and Mix experiments are similar in distribution and magnitude for temperature, humidity, and wind respectively. Temperature impacts are greatest in the upper troposphere and stratosphere, particularly in the Tropics. The Mix experiment has greater beneficial temperature impact in the Tropics than the Polar experiment, while the Polar experiment has more beneficial impact than the Mix experiment near the poles, especially the south pole, as expected from the large difference in numbers of RO observations at high and low latitudes (Figure 2).

Some areas of degradation are noted in the extratropics below 500 hPa; this has been seen in previous OSSE experiments and is described in detail in (Privé et al., 2022).

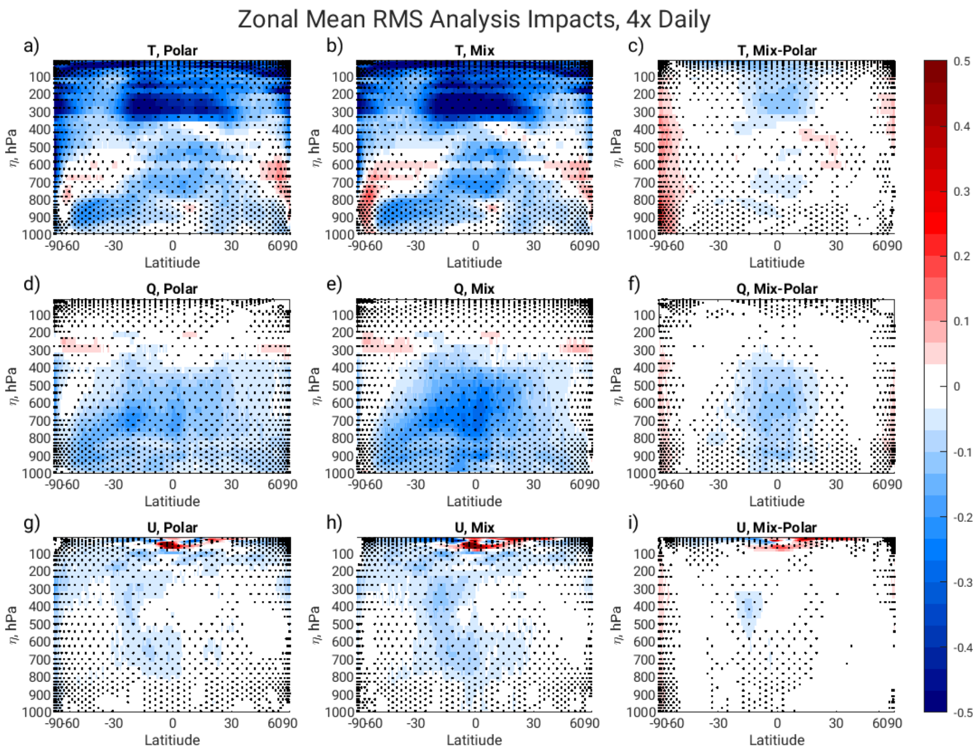

Figure 3. Zonal mean $RMSE_N$ (unitless fraction) for analysis fields, normalized by the Control analysis error fields, July-September. Top row, temperature; center row, specific humidity (shown below 200 hPa only); bottom row, zonal wind. Left column, Polar experiment; center column, Mix experiment; right column, difference between Mix and Polar experiments. Stippling indicates 95th percentile significance using paired two-tailed student's t-test.

The degradation at the lowest levels is largely in the form of the introduction of temperature biases by the RO data (not shown) over polar marine areas that have a strong temperature inversion in the boundary layer. The cause of the bias is not understood, but may involve differences between the two-dimensional ROPP operator used to simulate the bending angles and the one-dimensional NBAM operator used to ingest the data. Another possibility is small errors in the coefficients in the equation for refractivity, especially the k_1 coefficient for the "dry" term; experiments with large numbers of RO data in the Radio Occultation Modeling Experiment (ROMEX, Anthes et al., 2024) have shown great sensitivity in several different models' biases due to small (0.05%) changes in k_1 (Shao et al., 2025).

The mid-tropospheric degradation in the extratropics is related to an increase in the analysis error variance rather than the bias. This type of degradation usually indicates that there is a mismatch between the assigned error weighting in the DAS and the actual observation error. Optimizing the assigned observation errors is an area of current research that is beyond the scope of this paper.

Maps of $\Delta RMSE$ between experiments and Control for the temperature analysis are shown for select levels in Figure 4. Blue color indicates that the experiment has less analysis error than the Control for the left and center columns, while for the right column, blue indicates less error for the Mix experiment compared to Polar. Note that values of $\Delta RMSE$ are not normalized, and are in units of K. In the stratosphere (top row), RO impacts are relatively uniform, particularly for the Mix experiment. In contrast, the Polar experiment has weaker beneficial impacts in the Tropics and similar beneficial impacts in the midlatitudes and near the poles in the stratosphere compared to Mix (Figure 4c). In the upper troposphere (center row), impacts are strongly beneficial across the Tropics, with better impacts in the deep Tropics in the Mix experiment. There are only small impacts over North America, Europe, and parts of Asia, likely due to the density of in situ observations such as rawinsondes and aircraft in these regions. At the 250 hPa level, the Polar experiment has more beneficial impact than the Mix experiment in the polar regions.

At lower levels (Figure 4, bottom row), the impacts are complicated, with degradation due to RO observations over some land regions, Antarctica, and near the ITCZ in the Indian Ocean, which are primarily due to induced temperature biases (not shown). Beneficial temperature impacts are seen at low levels over subtropical and extratropical oceans. In the Antarctic region, a higher density of RO in the Polar experiment results in near-neutral impacts, while in the more sparsely observed Mix experiment there is substantial degradation, particularly over sea ice.

Humidity impacts are beneficial for both the Polar and Mix experiments below 300 hPa as seen in Figure 3. The RO observations do not contain useful humidity information above 200 hPa, so the stratospheric impacts are not shown. In the troposphere, the difference in impacts between the Mix and Polar experiments for humidity follows the difference in observation concentration, with stronger beneficial impacts in the Tropics in the Mix experiment and stronger beneficial impacts in the Polar experiments at the poles.

Figure 5 shows maps of the RO impact on specific humidity at the 850 hPa level. As specific humidity itself has a strong latitudinal gradient, both $\Delta RMSE$ (top row) and the normalized $RMSE_N$ (bottom row) are shown. While the temperature impacts at this level were mixed, the humidity impacts are beneficial over almost the entire globe. The large impacts over the tropical Atlantic are important for tropical cyclogenesis. The Polar experiment outperforms the Mix experiment near the poles, while the Mix experiment is more impactful over the Tropics, especially in localized areas over the eastern Pacific, eastern Atlantic, and Indian oceans.

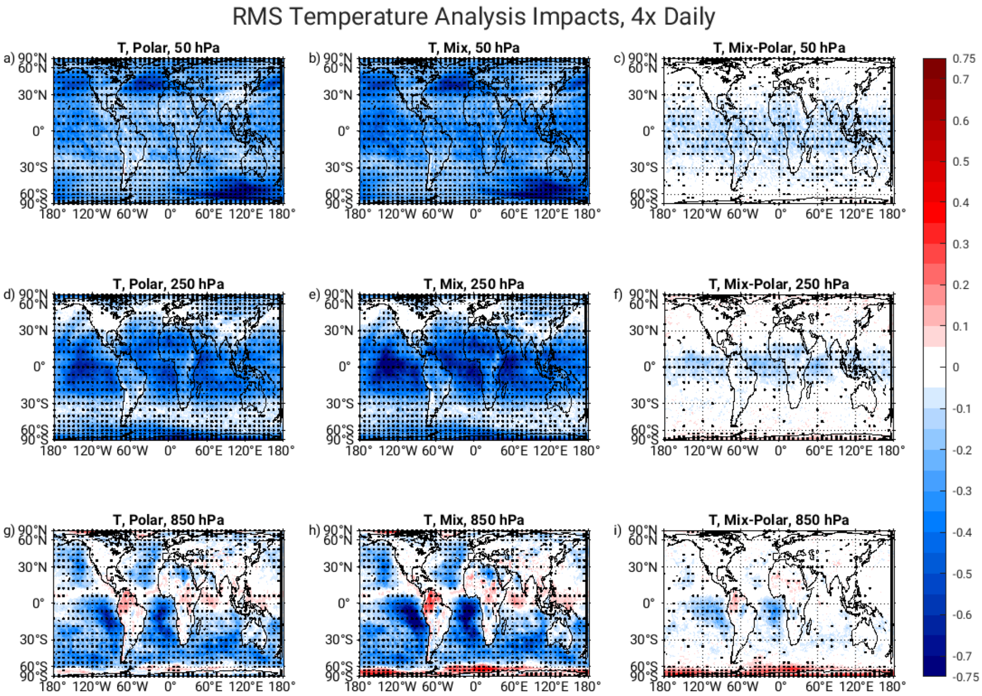

Figure 4. $RMSE_{Exp}$ -$RMSE_{Control}$ for analysis temperatures, July-September, K. Top row, 50 hPa; center row, 250 hPa; bottom row, 850 hPa. Left column, Polar experiment; center column, Mix experiment; right column, $RMSE_{Mix} - RMSE_{Polar}$. Stippling indicates 95th percentile significance using paired two-tailed student's t-test.

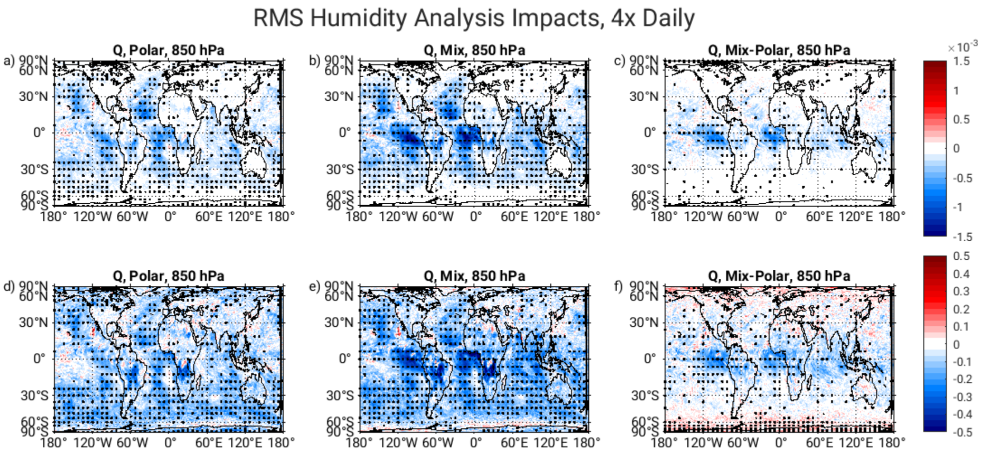

Figure 5. $RMSE_{Exp}$-$RMSE_{Control}$ for analysis specific humidity at 850 hPa, July-September. Top row, non-normalized $\Delta RMSE$, $kg\,kg^{-1}$; bottom row, $RMSE_N$ (unitless fraction). Left column, Polar experiment; center column, Mix experiment; right column, difference between Mix and Polar experiments. Stippling indicates 95th percentile significance using paired two-tailed student's t-test.

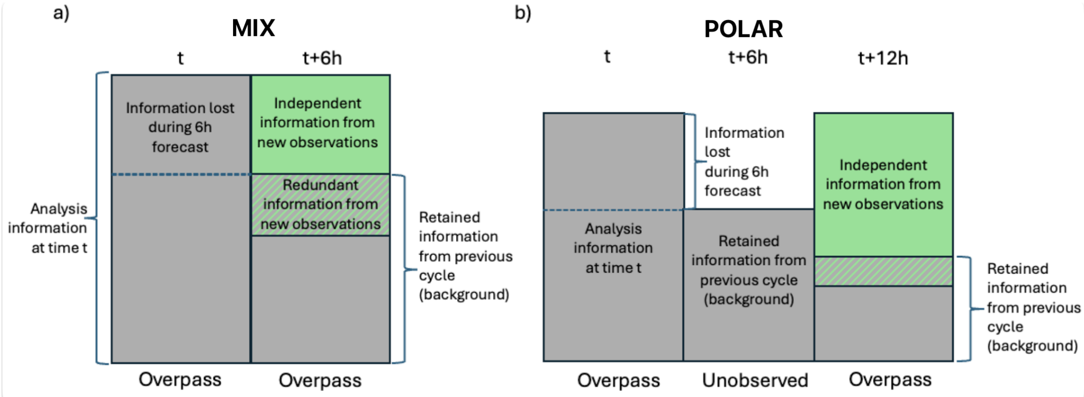

Figure 6. Schematic diagram showing the total information from RO in the analysis of two consecutive cycles at t and $t + 6h$ for a) the Mix experiment and b) for three cycles for the Polar experiment. The independent new information obtained from observations is indicated by green areas, the retained background information is indicated by grey areas, and the observation information that is redundant with retained background information is in hatched green and grey.

Overall, the differences between the Polar and Mix experiments are largely explained by considering the difference in the observation distribution along with the sensitivity of the system to the addition of RO data given the current data assimilation system and global observing network. The Mix experiment impacts, with nearly uniformly distributed RO observations, give an estimate of the location of areas of sensitivity. The Tropics are particularly sensitive to the addition of RO, especially in the upper troposphere and stratosphere for temperature and the mid troposphere for humidity and zonal wind. Antarctica is also a local region of sensitivity due to the high surface altitudes and model difficulties in accurately representing the extreme conditions. Due to the large geographic extent of the Tropics, the Mix experiment outperforms the Polar experiment when considered globally due to the greater number of RO observations near the equator.

3.2 Cycle Time Impacts

While the overall impact of RO in the Polar and Mix experiments has been shown to depend largely on the number and spatial distribution of the RO data, there is an additional question of the role of temporal frequency of the observations (refresh rate). In the Mix experiment, RO spatial coverage is relatively uniform in time, as illustrated by comparing the daily means and 0000 and 1800 UTC observation distributions in the bottom row of Figure 2. In the Polar experiment, most areas are more densely observed when there is an overpass of the orbit, but are observed only at 12 hour intervals, i.e. at every other cycle time for a 6-hour DAS window.

Retention of information from previous observations and addition of independent information obtained from the new observations both contribute to the necessary refresh rates. Retention of information depends on how quickly observational information is lost during the 6-h forecast interval between analysis cycles. When the information is well retained, a more frequent refresh rate is less important. The left panel in Figure 6 compares the information in the analyses at two consecutive cycles for the Mix case, at times t and t+6h, assuming the information content is roughly the same for the two cycles. During the 6-h forecast period, some information is lost through error growth. The 6-h forecast initiated at time t is used for the background in the t+6h analysis. The observations ingested for the t+6h cycle contain some information that is redundant (green and grey hatching in Figure 6) with the retained background information (grey area) and

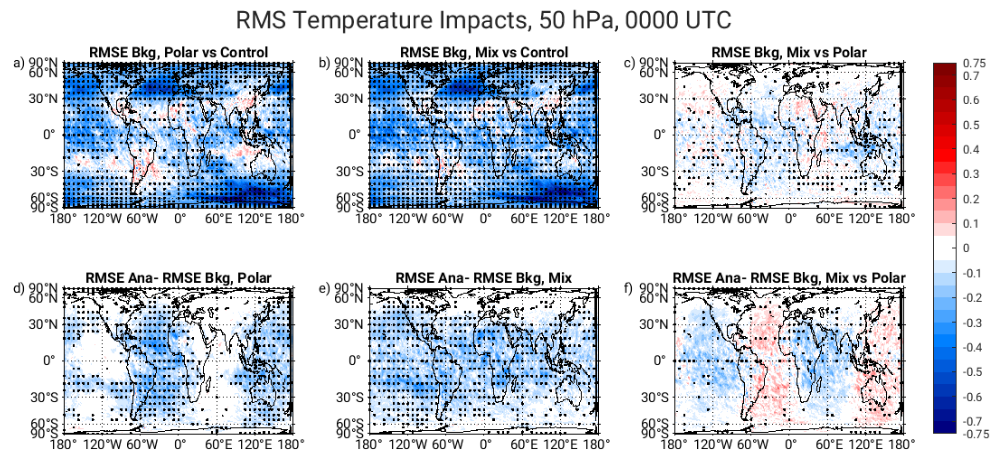

Figure 7. Temperature RMSE differences at 50 hPa for the 0000 UTC cycle time, units of K. Top row, a,b) difference in background RMSE between experiment and Control, c) difference in background RMSE between Mix and Polar. Bottom row, RMSE difference between analysis and background. Left column, Polar experiment; center column, Mix experiment; right column, Mix minus Polar. Stippling indicates 95th percentile significance using paired two-tailed student's t-test.

some new independent information (solid green). In the Polar case represented in Figure 6b, no RO observations are locally ingested at the $t{+}6h$ cycle time, so more background RO information is lost prior to the next ingestion of RO observations at $t{+}12h$.

The magnitude and distribution of retained RO information from one cycle to the next may be estimated by comparing the background error in the Cycling experiments with that of the Control (top row of Figure 7 for 50 hPa temperature). If no RO information were retained between 6-hour cycle times, the background in the Cycling experiments would be similar to that of the Control. The difference between the experiment background RMSE and Control background RMSE is a measure of the retained RO information. Figure 7a,b indicates large background impacts versus Control for both the Polar and the Mix experiments especially in the extratropics, indicating a large retention of information in both experiments. It is notable that in the Polar experiment, background improvements are seen in areas that have not been overpassed in 12 h (Figure 7a), implying that information is fairly well retained at this timescale. The difference of the background errors between the Mix and Polar experiments in Figure 7c indicates slightly better retention of information in the Mix experiment in most of the tropics.

Also shown in Figure 7 (bottom row) are the differences between the analysis RMSE and the background RMSE for the Polar (7d), Mix (7e) and Mix minus Polar (7f) experiments. Note that this metric includes both impacts of RO and all other ingested data types; however, the impact of observations other than RO are small at 50 hPa. The Polar (7d) and the Mix minus Polar (7f) differences clearly reflect the difference in RO orbits. Under the orbits of the Polar experiment the observations have greater impact than the fewer observations in the Mix experiment (pink areas in 7f), particularly in the tropics, although the difference is largely not statistically significant. However, this greater observation information content translates to relatively small improvements in the analysis, as shown in Figure 8g, which shows the differences in the analysis impacts of the Mix minus Polar Cycling experiments.

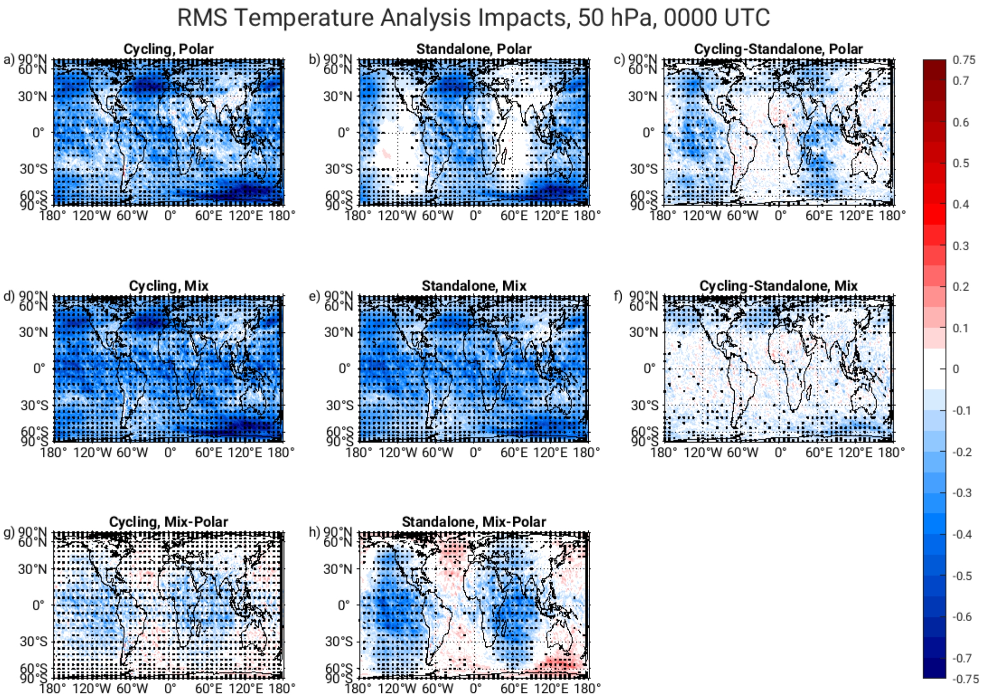

Figure 8. $RMSE_{Exp}$-$RMSE_{Control}$ for analysis temperatures at 50 hPa (K), July-September. All calculations are for the 0000 UTC cycle time only. Top row, Polar experiment; center row, Mix experiment; bottom row, difference between Mix and Polar experiments. Left column, full Cycling experiment; center column, Standalone experiment; right column, difference between Cycling and Standalone experiments. Stippling indicates 95th percentile significance using paired two-tailed student's t-test.

Figure 8 illustrates the Cycling and Standalone analysis impacts for the Polar and Mix experiments and their differences (top two rows) and the differences between the Mix and Polar for Cycling and Standalone experiments (bottom row) for temperature at 50 hPa. As mentioned above, the new observations ingested during an analysis cycle contain some information that is redundant with the retained information (the background) and some new, independent information. The total (redundant plus independent) information in the new observations is given by the Standalone reduction in RMSE (Figure 8b and 8e). Recall that in the Cycling case, RO information accumulates in the background, but in the Standalone case, the background state is taken from the Control in which no RO are ingested. The difference between RMSE between the experiment and the Control analysis isolates the total information from the new RO observations (the green area in Figure 6 plus the redundant information in green/grey hatching).

The difference between Standalone analysis impacts for the Mix and Polar experiments is shown in 8h, illustrating the relative observation information content in the two experiments for a single cycle time. As expected, the Polar experiment has more new observation information from RO than the Mix experiment (pink areas in Figure 8h) under the orbital swath with the exception of the equatorial region. Comparing Figure 8g and 8h indicates that there is less difference between Mix and Polar analyses in the presence of retained RO information (Figure 8g) than when retained RO information is excluded (Figure 8h).

The difference between the Cycling and Standalone analysis impacts for each experiment illustrates the amount of retained background RO information that is not redundant with the RO observations. There is a clear difference in the distribution of RO analysis impacts between the Cycling and Standalone cases for the Polar (Figure 8c) experiment, where the retained background information is evident in areas not currently overpassed, as well as to a lesser degree in the north Atlantic region. In the Mix experiment (Figure 8f), the difference between Cycling and Standalone is small in the tropics but more substantial in the midlatitudes, indicating that the RO observation information content in the extratropics may be more independent of the retained background information than in the tropics.

We looked at similar differences in backgrounds (not shown) and analyses for temperature at 250 hPa and specific humidity (not shown) at 850 hPa. In both cases both the Polar and Mix experiments show a large retention of information from previous cycles, especially in the tropics, in contrast to the stronger retention of information in the midlatitudes at 50 hPa. The Cycling analysis impacts for temperature at 250 hPa are shown in Figure 9, highlighting the dominance of the tropical impacts. Further breakdown of the temperature impacts of RO in the tropics into mean (bias) and standard deviation of errors indicates the persistent improvements in temperature at 250 hPa are associated with smaller biases. Unlike at 50 hPa, the Polar overpass region is not as clearly delineated at 250 hPa in the difference between Mix and Polar impacts.

The results from these experiments show that 14,000 RO profiles per day make a large positive impact on analyses and forecasts for both the Polar and the Mix distributions. Substantial amounts of information are retained from previous assimilation cycles, and this retained information is greater in magnitude than the new information provided in both the Mix and Polar experiments. They also show that the Mix experiment performance is better in most respects than the Polar experiment. The differences vary with altitude and latitude and are somewhat different for temperature and water vapor. The improvement of Mix versus Polar depends on how well information from previous observations is retained in the analyses. When the information is well retained for more than six hours, a rapid refresh rate is less important. When the information is lost quickly, as in regions of rapid error growth, a rapid refresh rate is much more beneficial.

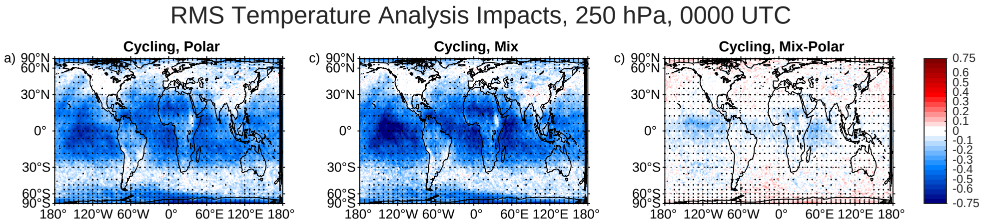

Figure 9. $RMSE_{Exp}$-$RMSE_{Control}$ for analysis temperatures at 250 hPa, July-September, units of K. All calculations are for the 0000 UTC cycle time only. Left, Polar experiment; center, Mix experiment; right, difference between Mix and Polar. Stippling indicates 95th percentile significance using paired two-tailed student's t-test.

4 Forecast Impacts

It is instructive to examine the short-term forecast impacts in comparison to the analysis impacts of RO to evaluate the regional evolution of observational information at timescales longer than the 6-h intervals previously discussed. Short term forecast impacts are calculated for the 24-h forecasts for temperature on select levels in Figure 10 for the 0000 UTC cycle time.

Comparing the 50 hPa impacts for the analysis (left columns in Figure 8) to the 24-h forecast impacts (top row Figure 10), several features stand out. First, the extratropical impacts appear fairly similar while the tropical impacts are much weaker in the forecast than the analysis. Also, the orbital swath visible in the analysis impact difference between Mix and Polar (Figure 8g) is not apparent in the comparison of Mix and Polar forecast impacts (Figure 10c). These differences between the analysis and forecast impacts imply that in the stratosphere, the observation information in the Tropics is more rapidly lost than in the midlatitudes.

At 250 hPa, a similar comparison between Figure 9 and the bottom row of Figure 10 shows more congruence between the 24-h forecast impact and the analysis impacts in the upper troposphere compared to the stratosphere. Large forecast impacts are still seen in the Tropics, particularly in the east and central Pacific, Atlantic, and Indian Ocean regions. There are select areas of the Tropics where impacts are near zero in the forecast but more beneficial in the analysis, such as equatorial Africa, the Amazon basin, and off the southwest coast of Mexico and central America - these are areas of deep convection where physical and dynamical processes in the forecast model may result in destruction of information. In the southern hemisphere midlatitudes, the RO forecast impacts are mostly neutral, rather than the mildly beneficial impacts seen for the analysis. However, some areas of the north Atlantic and Pacific that did not show statistically significant benefits for the analysis do show significant improvement at 24 hours.

Unlike in the stratosphere, in the upper troposphere (250 hPa) the difference between the Mix and Polar experiment forecast impacts still shows evidence of the influence of the orbital overpass in the Polar experiment, as evidenced by Figure 10f. The difference between Mix and Polar is clear in both the analysis impact (Figure 9c) and forecast impact (Figure 10f), and the small advantage to the Mix experiment over the eastern Pacific and Indian ocean areas that were not overpassed in the Polar experiment can still be seen. It is notable that while for the analysis impacts the advantage in the Mix experiment is confined to the deep Tropics close to the equator, for the forecast im-

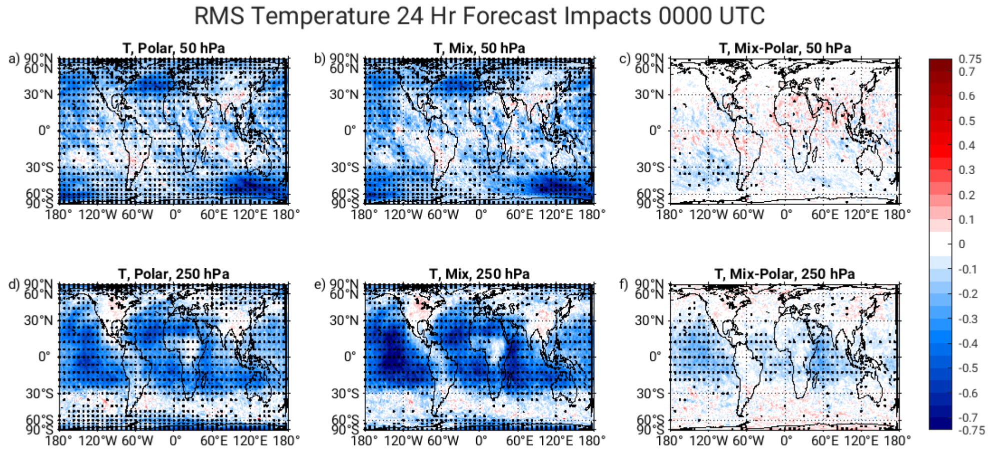

Figure 10. $\Delta RMSE$ for 24-h forecast temperatures at 0000 UTC, K. Top row, 50 hPa; bottom row, 250 hPa. Left column, Polar experiment; center column, Mix experiment; right column, difference between Mix and Polar experiments. Stippling indicates 95th percentile significance using paired two-tailed student's t-test.

pacts the Mix advantage over Polar is more evenly spread from 30S-30N. These areas of greater benefit from the Mix experiment occur in the gaps between the Polar experiment orbit.

Medium-range forecast impacts are helpful to estimate the lifespan of retained RO information. Regional calculations of $RMSE_N$ temperature forecast impacts out to seven days are shown in Figure 11 for three regions: 20N-90N (Northern hemisphere extratropics, NHEX), 20S-90S (Southern hemisphere extratropics, SHEX), and 20S-20N (Tropics). In the NHEX region, there is minimal difference in RO impact between the Mix and Polar experiments, with both having initially strong beneficial impacts in the upper troposphere that last for 3-5 days, and weaker but more persistent beneficial impacts in the lower troposphere. In the SHEX, the Polar experiment outperforms the Mix experiment (pink colors in Figure 11h) in the mid and lower troposphere for the first 2-3 days of the forecast. Both experiments have beneficial impacts in the upper and lower troposphere of the SHEX that persist for 4-5 days, although weak degradation develops in the mid troposphere after an initial period of improvement.

The Tropics has a similar pattern of temperature forecast impacts to the NHEX, with strong beneficial impacts in the upper troposphere that dissipate after 3 days, and weaker but more persistent beneficial impacts in the lower troposphere (Figure 11c,f,i). However, the upper troposphere impacts become detrimental after day 3, and there is a significant advantage for the Mix experiment compared to the Polar experiment in both the upper and lower troposphere.

Initially beneficial RO impacts in the Tropics that become detrimental after 2-4 days have been observed in previous OSSE studies (Privé et al., 2022). The temperature forecast degradation in the Tropics after day 3 is related to a temperature bias in which the entire column (not shown) is cooled - this is beneficial below 500 hPa but detrimental at higher levels. While initially the upper troposphere is warmer for the RO experiment cases, reducing the bias compared to Control, the upper level temperatures decrease steadily as the forecast progresses. After day 3, the Control begins to slowly warm at upper levels, but the Mix and Polar cases continue to cool until day 5, resulting in

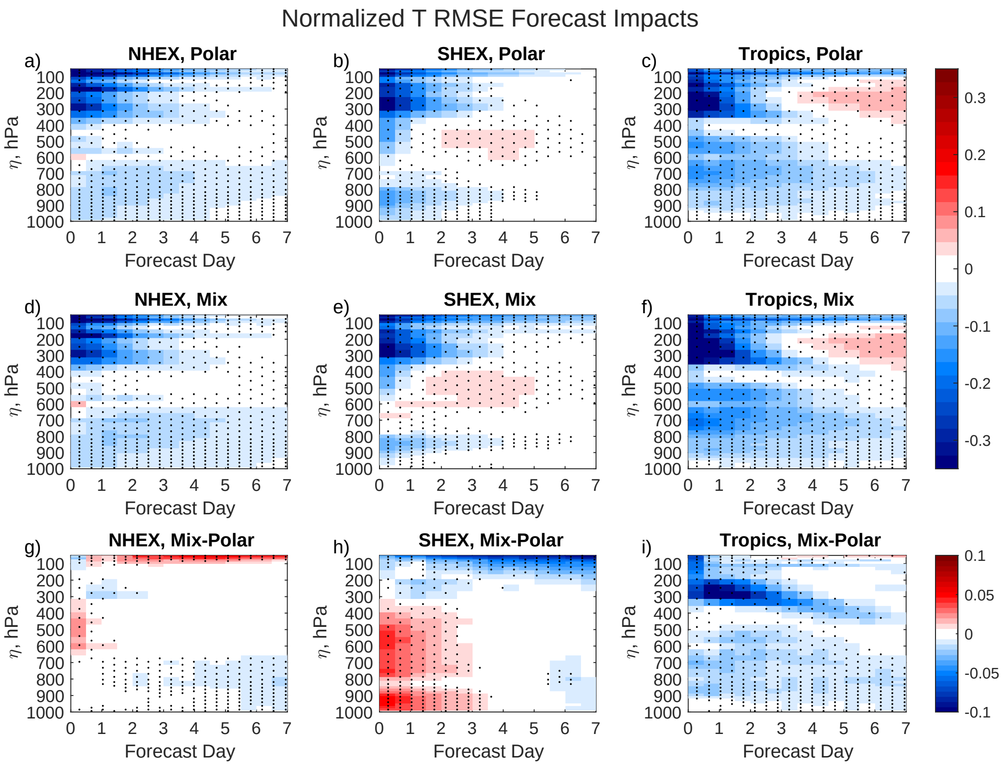

Figure 11. Regional $RMSE_N$ (unitless fraction) for 7 day forecast temperatures initialized at 0000 UTC. Stippling indicates statistical significance at the 90% level. Top row, Polar experiment; center row, Mix experiment; bottom row, Mix - Polar experiments. Left column, NHEX region; center column, SHEX region; right column, Tropics.

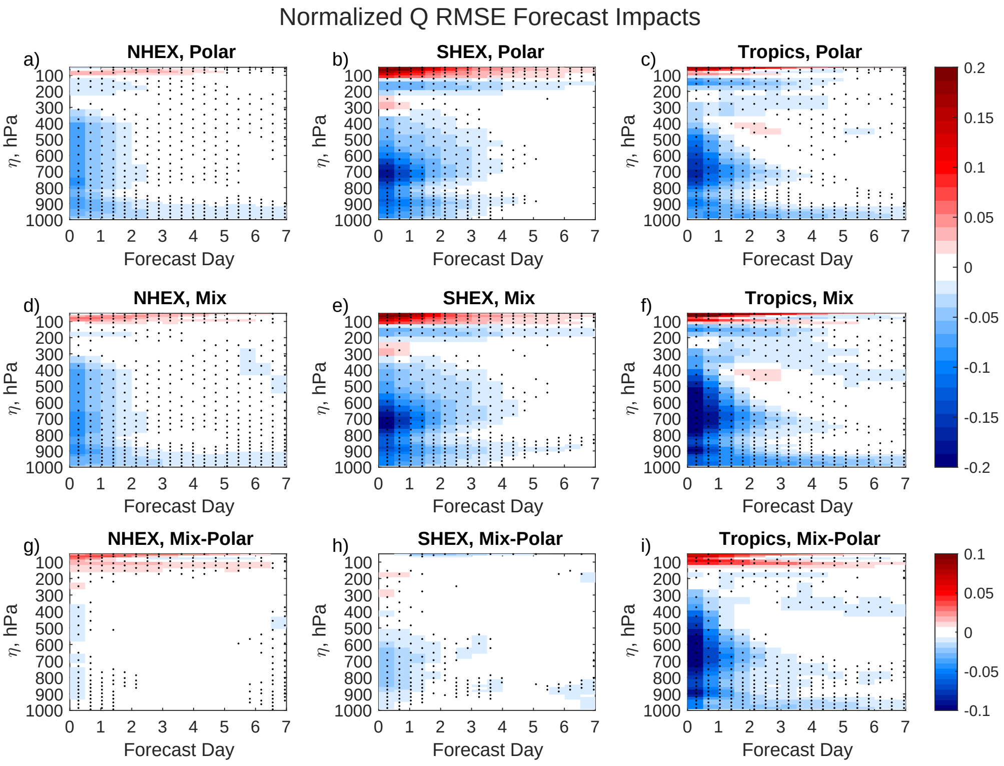

Figure 12. As in Figure 11, but for specific humidity (unitless fraction).

greater bias compared to Control. This degradation is believed to be due to a deep convective response that is triggered by the assimilation of observations in sensitive areas such as the West Pacific. This difference in bias is greater than the improvement to the error standard deviation (not shown) caused by the ingestion of RO, which still favors the experiments compared to Control.

Forecast impacts for specific humidity are shown in Figure 12. In the troposphere, significant RO impacts on humidity persist into the medium range forecast, with extended impacts noted near the surface. In the NHEX, there is little difference between impacts for Mix and Polar, as seen for temperature. However, for the SHEX, there is an advantage for the Mix experiment during the early forecast period in the lower troposphere. For the Tropics, the strong initial impact fades quickly in the mid troposphere, but persists longer in the lower troposphere, with much greater impacts in Mix compared to Polar. These improvements in the lower tropospheric specific humidity forecasts are expected to improve forecasts of precipitation and tropical storm development.

5 Forecast Sensitivity Observation Impacts (FSOI)

FSOI uses a linearized version, or adjoint, of the forecast model to estimate the simultaneous impacts of all ingested observation types by a single metric of forecast skill. The GEOS/GSI adjoint includes linearization of moist convective processes, so is considered a 'moist' adjoint (Holdaway et al., 2014). Because the linearization is only valid for short-range forecasts, FSOI is generally used on the 24-h forecast. Here, the choice of metric is the global 24-h total wet energy error norm, calculated using the NR for verification. The total wet energy error norm includes contributions from temperature, mois-

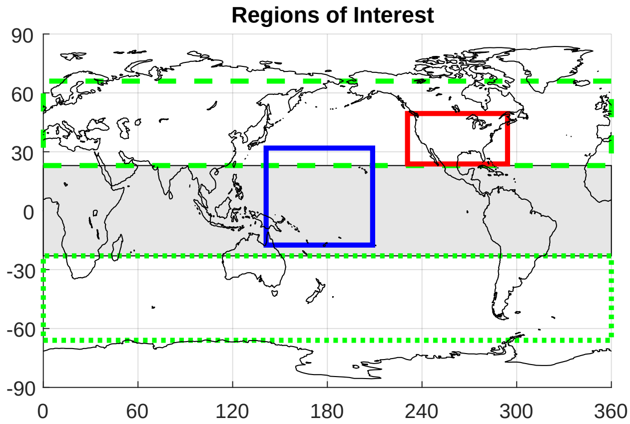

Figure 13. Subregions examined with FSOI. Green dashed box, NHM; green dotted box, SHM; light grey filled box, Tropics; blue box, West Pacific; red box, CONUS.

ture, and wind errors. FSOI statistics are calculated for multiple subregions as illustrated in Figure 13. Negative FSOI values indicate a reduction in the 24-h forecast error due to the ingestion of observations.

Figure 14 shows the FSOI estimates of mean observation impacts per cycle for all ingested observation types in the Polar and Mix experiments, calculated using four cycle times per day. In the northern hemisphere midlatitudes (NHM), RO contributes approximately 10% of the total observation impact, ranking similar to the impact of two combined IASI or two combined ATMS platforms. The Mix experiment has a slightly greater impact of RO than the Polar experiment in the NHM region. In the southern hemisphere midlatitudes (SHM), RO accounts for 13-14% of the total observation impact, with slightly greater impact in Polar compared to Mix. For the SHM region, RO impacts fall between the hyperspectral IR platforms (CrIS-FSR and IASI) and the ATMS and AMSU-A microwave platforms.

In the Tropics, there is a large difference in RO impact for the Mix and Polar experiments, with RO contributing 26% of the total impact for Mix but only 16% of the impact in Polar. RO observations have the second largest impacts of all data types in the Polar experiment, and the largest impacts in the Mix experiment. Notably, the data types other than RO have weaker impacts in the Mix experiment compared to the Polar experiment. The strong improvements to the background state in the Mix experiment as noted in section 3.2 are the likely cause of this weakening of impacts in the Mix experiment, leaving less 'work' for the observations to perform. The large fraction of the earth covered by the Tropics results in stronger RO impacts globally for Mix compared to Polar.

For subregions that are intermittently overpassed in the Polar experiment, the FSOI at different cycle times illustrates the local variability of RO impacts, particularly for the Polar experiment. In the West Pacific region (blue box in Figure 13), RO in the Mix experiment is consistently one of the top two most impactful data types along with AMVs as shown in Figure 15. For overpasses of the Polar orbit at 0000 and 1200 UTC, the RO FSOI is similar in magnitude to that of the Mix experiment, but at 0600 and 1800 UTC the Polar orbit does not directly overpass and the local impacts are much smaller because fewer observations occur within the subregion. FSOI only considers the impact of observation types ingested during the current cycle, not impacts of observations ingested at prior cycles. The variability of FSOI with cycle time in the Mix experiment can be

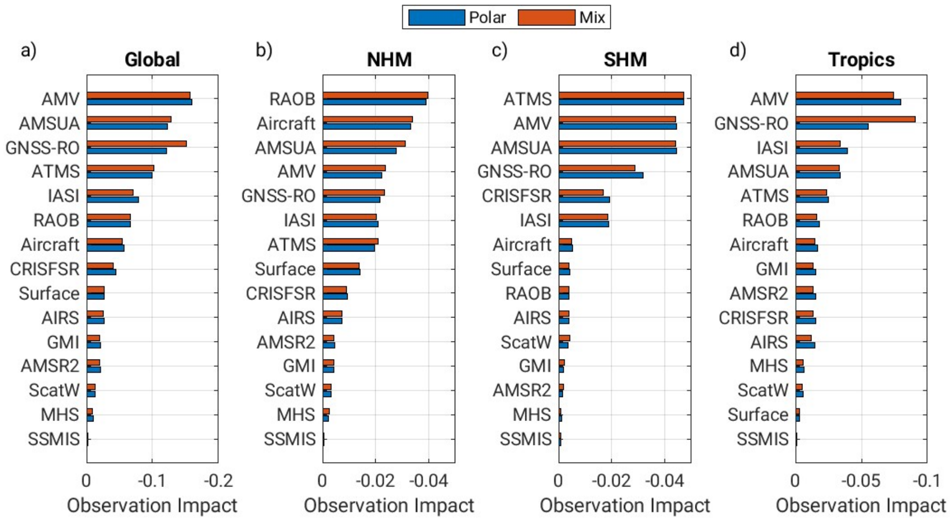

Figure 14. FSOI estimates of observation impact on the 24-h total wet energy norm for observations in subregions, mean impact per cycle calculated from July-September using four times daily calculations ($J\,kg^{-1}$).

due to the local diurnal cycles along with the availability of other data types such of rawinsondes and aircraft.

One area of particular interest is the conterminous United States, represented by the red CONUS box in Figure 13. CONUS is very well observed with extensive in-situ observations from surface stations, rawinsondes, and aircraft. However, rawinsondes are predominantly available only at 0000 and 1200 UTC, and aircraft have a strong diurnal cycle of availability with minimum at the 0600 UTC cycle time. The Polar experiment overpasses CONUS most directly at 1800 UTC, at which cycle time the RO for Polar has slightly more impact than for the Mix experiment. At the other cycle times, the Mix experiment is more impactful, with large differences at 0000 and 1200 UTC when the Polar orbit has little coverage of CONUS, and a smaller difference at 0600 UTC when the Polar orbit overpasses but has less total coverage than at 1800 UTC.

6 Summary and Discussion

We have compared the impact on NWP of two constellations providing RO observations, one a polar-only orbiting constellation and another with the same number (14,000 profiles per day), but with a mixture of polar and equatorial orbits in observing system simulation experiments (OSSEs). Over the period of a day, the mixed constellation provides denser observations in the tropics and subtropics and samples all local times, while the polar constellation provides denser observations in middle and high latitudes, but has 6-h gaps in the local time coverage. We examined the reduction in RMS errors in temperatures and water vapor and the forecast sensitivity to observation impacts (FSOI) in the analyses and forecasts globally and for different regions.

The setup of the NWP data assimilation system includes analyses generated every six hours. In the Mix experiment locations are sampled during every analysis cycle, but most locations in the Polar experiment are sampled every other cycle.

Our results show that the assimilation of 14,000 RO profiles per day significantly improves analyses and short- and medium-range global forecasts regardless of refresh rates,

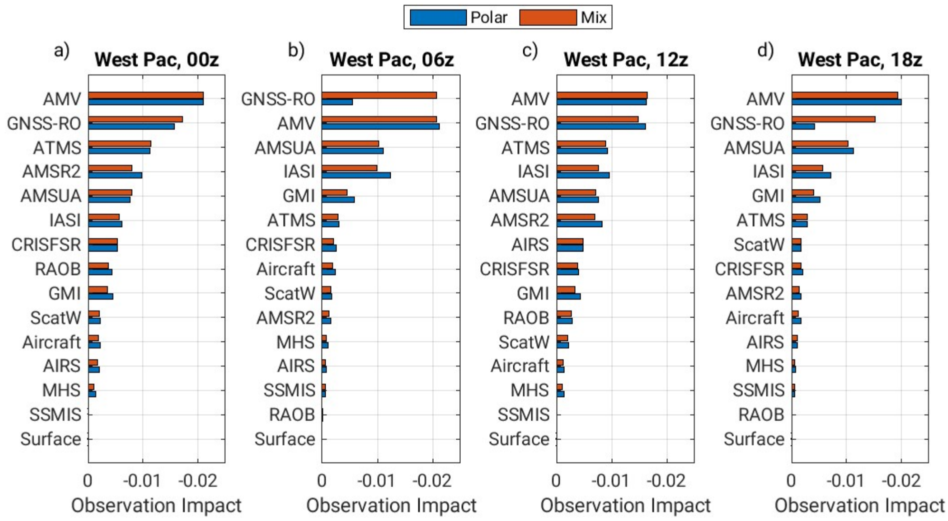

Figure 15. FSOI estimates of observation impact on the 24-h total wet energy norm for observations in the west Pacific subregion, mean impact per cycle calculated from July-September for 0000, 0600, 1200, and 1800 UTC cycle times ($J\,kg^{-1}$).

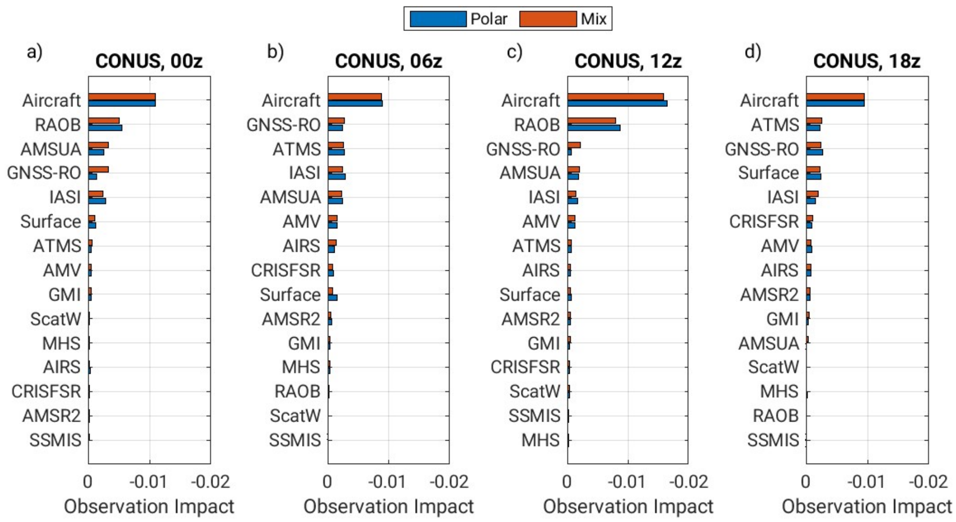

Figure 16. FSOI estimates of observation impact on the 24-h total wet energy norm for observations in the CONUS region, mean impact per cycle calculated from July-September for 0000, 0600, 1200, and 1800 UTC cycle times ($J\,kg^{-1}$).

with RO observations ranked between second and fifth in impact compared to other observations, confirming numerous previous studies. The new results show that there are advantages to a constellation with a mixture of polar and equatorial orbits compared to a constellation with polar only orbits. These advantages depend on latitude and altitude, and are somewhat different for temperature, water vapor and wind. The tropical upper troposphere is particularly sensitive to the addition of RO observations, and the advantages to the Mix experiment are found in the tropics at all altitudes for temperature and the lower troposphere at all latitudes for water vapor.

We show how the impact of the different refresh rates depends on the retention time scales of the observation impacts. The question of how frequently the atmosphere should be observed depends on how well the model retains the information from the assimilated observations. If the observational information is well retained and if forecast error growth is relatively slow, the repeat interval of observations (refresh rate) does not need to be as frequent. However, if there is a rapid loss of information due to rapid error growth (as in regions of rapid tropical or extratropical cyclone development), more frequent repeat observations are necessary.

These experiments indicate that for most regions, the RO information is fairly well retained over six hours. Therefore, the RO impacts are largely a function of the daily observational density (number of observations and horizontal resolution) along with the underlying capacity of the observations to improve the analysis state. The Mix experiment is generally superior to the Polar experiment due to the denser coverage of the particularly sensitive Tropics.

In the polar-only experiment, densely spaced observations are received in 90° longitude bands every 6 hours, with no observations received in these bands during the next 6 hours. During the period when observations are available locally, the resulting analysis is improved and some of these improvements are retained in the background state of during the next assimilation cycles. However, during the period when no observations are received, there is no additional improvement in the analysis. The overall result is a leapfrog situation in which for extratropical regions, the Polar-only experiment outperforms the Mix experiment during the cycle in which a large number of observations are obtained, but then falls behind during the next cycle when there are no RO observations. When all cycles are combined, the difference between Mix and Polar is nearly neutral in midlatitudes. The Polar case has an advantage over the Mix case near the poles, where there is a high density of observations in the Polar experiment.

The forecast impacts illustrate the timescale for retention of the RO information and demonstrate complex behaviors for different regions, altitudes, and model variables. Some RO information is retained in temperatures throughout the 7-day forecast in the upper-troposphere-lower-stratosphere and the lower troposphere in both the Northern and Southern hemispheres. For specific humidity, the improvement occurs in the middle and lower troposphere and persists for about 4 days.

One limitation of this study is the evaluation of only a single season. As the northern hemisphere is more densely observed by in situ instruments, some differences would be expected if boreal winter were evaluated rather than austral winter. In boreal winter, the enhanced RO impacts might be expected in areas of strong baroclinic growth, such as over the north Atlantic and north Pacific basins. The Polar scenario would be anticipated to have a more beneficial impact in the northern hemisphere extratropics compared to the southern hemisphere extratropics during boreal winter. However, the well-observed continental areas in the northern hemisphere may not be as strongly impacted by RO observations compared to the southern hemisphere ocean in winter as the background error over the boreal continents is quite low.

It should be noted that the rate of error growth is generally considered to be fastest at small scales and in regions of atmospheric instabilities. In order to resolve small-scale features, more frequent repeat intervals are required to compensate for rapid information destruction at these scales. Such high-impact cases include regions of rapid extra-tropical or tropical storm development, where frequent and timely observations are most needed. In cases where model error growth rapidly destroys observation information, the question might be asked as to whether frequent observations are actually useful as the information will not be retained in the forecasts after a short time. However, improving the analysis state is a useful goal, especially now as new AI models use analyses, re-analyses, and direct observation as training datasets.

Open Research Section

The full GEOS-5 Nature Run Global Modeling and Assimilation Office, NASA (2014) is available for download from a portal at `https://gmao.gsfc.nasa.gov/gmao-products/7km-g5nr/`

The codes used to generate simulated observations are available on zenodo at `https://doi.org/10.5281/zenodo.11387384`

The GEOS/GSI version used for the experiment runs is available on zenodo at `https://doi.org/10.5281/zenodo.11387002`

Conflict of Interest disclosure

The authors declare there are no conflicts of interest for this manuscript.

Acknowledgments
The authors would like to thank Ron Errico (retired) for his longstanding efforts in developing the GMAO OSSE framework, and most recently in implementing the simulated all-sky observation types used in this manuscript. Support for this project was provided by NASA Goddard Space Flight Center (GSFC) and the Analysis of Alternatives project in NOAA/NESDIS. Resources supporting this work were provided by the NASA High-End Computing (HEC) Program through the NASA Center for Climate Simulation (NCCS) at GSFC. The software for simulating GNSS-RO observations was provided by the Radio Occultation Processing Package (ROPP) of the Radio Occultation Meteorology (ROM) Satellite Applications Facility (SAF) of EUMETSAT, with the assistance of Sean Healy at ECMWF. The Claude LLM was used to review the accuracy of equations used in the text. Two anonymous reviewers provided comments that lead to improvements in this manuscript.

References

Anthes, R., Maier, M., Ackerman, S., Callahan, R. A. L. W., Dittberner, G., Edwing, R., . . . Yoe, J. G. (2019). Developing priority observational requirements from space using multi-attribute utility theory. *Bull. of the Amer. Met. Soc.*, *100*, 1753–1774. doi: 10.1175/BAMS-D-18-0180.1

Anthes, R., Marquardt, C., Ruston, B., & Shao, H. (2024). Radio occultation modeling experiment (ROMEX)- determining the impact of radio occultation observations on numerical weather prediction. *Bull. of the Amer. Met. Soc.*, *105*. doi: 10.1175/BAMS-D-23-0326.1

Anthes, R., & Schreiner, W. (2019). Six new satellites watch the atmosphere over Earth's equator. *EOS*, *100*. doi: 10.1029/2019EO131779

Anthes, R., Sjoberg, J., Feng, X., & Syndergaard, S. (2022). Comparison of COS-

MIC and COSMIC-2 radio occultation refractivity and bending angle uncertainties with latitude in August 2006 and 2021. *Atmosphere*, *13*. doi: 10.3390/atmos13050790

Aparicio, J., & Deblonde, G. (2008). Impact of the assimilation of CHAMP refractivity profiles in Environment Canada global forecasts. *Mon. Wea. Rev.*, *136*, 257–275. doi: 10.1175/2007MWR1951.1

Atlas, R., & Emmitt, G. (2008). Review of observing system simulation experiments to evaluate the potential impact of lidar winds on numerical weather prediction. In *Ilrc24* (Vol. 2, pp. 725–729). (ISBN 978-0-615-21489-4)

Atlas, R., & Riishojgaard, L. (2008). Application of OSSEs to observing system design. In P. Ardanuy & J. Puschell (Eds.), *Remote sensing system engineering* (p. 9). doi: 7087:708707,doi:10.1117/12.795344

Boukabara, S.-A., Ide, K., Shahroudi, N., Zhou, Y., Zhu, T., Li, R., … Hoffman, R. (2018). Community Global Observing System Simulation Experiment (OSSE) Package (CGOP): perfect observations simulation validation. *J. Atmos. Ocean Tech.*, *35*, 207–226. (doi:10.1175/JTECH-D-17-0077.1)

Charney, J., Halem, M., & Jastrow, R. (1969). Use of incomplete historical data to infer the present state of the atmosphere. *J. Atmos. Sci.*, *26*, 1160–1163. doi: 10.1175/1520-0469(1969)026⟨1160:UOIHDT⟩2.0.CO;2.

Cucurull, L., Atlas, R., Li, R., Mueller, M., & Hoffman, R. (2018). An observing system simulation experiment with a constellation of radio occultation satellites. *Mon. Wea. Rev.*, *146*, 4247–4259. doi: 10.1175/mwr-d-18-0089.1

Cucurull, L., Casey, S., Vidal, A., & Lim, A. (2026). The value of radio occultation data in numerical weather prediction: An OSSE on the impact of profile volume, geographical distribution, and satellite bias correction. *Mon. Wea. Rev.*. (in review)

Cucurull, L., & Derber, J. (2008). Operational implementation of COSMIC observations into the NCEP's Global Data Assimilation System. *Wea. Forecasting*, *23*, 702–711. doi: 10.1175/2008WAF2007070.1

Cucurull, L., Derber, J., & Purser, R. J. (2013). A bending angle forward operator for global positioning system radio occultation measurements. *J. Geophys. Res.*, *118*, 14–28. doi: 10.1029/2012JD017782

Cucurull, L., & Mueller, M. (2020). An analysis of alternatives for the COSMIC-2 constellation in the context of global observing system simulation experiments. *Weather and Forecasting*, *35*, 51–66. doi: 10.1175/WAF-D-19-0185.1

di Tomaso, E., & Bormann, N. (2011). *Assimilation of ATOVS radiances at ECMWF: first year EUMETSAT fellowship report* (Tech. Rep.). ECMWF. (url: URL https://www.ecmwf.int/node/9049)

Errico, R., Privé, N., Carvalho, D., Sienkiewicz, M., Akkraoui, A. E., Guo, J., … Moradi, I. (2017). *Description of the GMAO OSSE for Weather Analysis software package: Version 3* (Tech. Rep. No. 48). National Aeronautics and Space Administration. (NASA/TM-2017-104606)

Errico, R. M., & Privé, N. C. (2018). Some general and fundamental requirements for designing observing system simulation experiments (osses). *WMO Rep. WWRP 2018-8*, 33 pp.

Errico, R. M., Yang, R., Privé, N., Tai, K.-S., Todling, R., Sienkiewicz, M., & Guo, J. (2013). Validation of version one of the Observing System Simulation Experiments at the Global Modeling and Assimilation Office. *Quart. J. Roy. Meteor. Soc.*, *139*, 1162–1178. doi: 10.1002/qj.2027

Eyre, J., & Weston, P. (2014). The impact of the temporal spacing of observations on analysis errors in an idealised data assimilation system. *Quart. J. Roy. Meteor. Soc.*, *140*, 1441–1452. doi: 10.1002/qj.2227

Gail, W., Gayl, I., & Zeng, X. (2025). A backbone architecture for government observing systems. *Bull. of the Amer. Met. Soc.*, *106*, E386–E393. doi: 10.1175/BAMS-D-24-0173.1

Gelaro, R., Putman, W. M., Pawson, S., Draper, C., Molod, A., Norris, P. M., ... Wargan, K. (2014). *Evaluation of the 7-km GEOS-5 nature run* (NASA/TM–2014-104606, No. 36). NASA.

Global Modeling and Assimilation Office, NASA. (2014). *GEOS-5 Nature Run, Ganymed Release* [dataset]. Retrieved from `https://gmao.gsfc.nasa.gov/global\_mesoscale/7km-G5NR/`

Han, Y., van Delst, P., Liu, Q., Weng, F., Yan, B., Treadon, R., & Derber, J. (2006). *JCSDA Community Radiative Transfer Model (CRTM) - version 1* (NOAA Tech. Report 122).

Healy, S., Eyre, J., Hamrud, M., & Thépaut, J.-N. (2007). Assimilating GPS radio occultation measurements with two-dimensional bending angle observation operators. *Quarterly Journal of the Royal Meteorological Society*, *133*(626). doi: 10.1002/qj.63

Healy, S., & Thépaut, J.-N. (2006). Assimilation experiments with CHAMP GPS radio occultation measurements. *Quart. J. Roy. Meteor. Soc.*, *132*, 605–623. doi: 10.1256/qj.04.182

Ho, S.-P., Anthes, R. A., Ao, C. O., Healy, S., Horanyi, A., Hunt, D., ... others (2020). The COSMIC/FORMOSAT-3 radio occultation mission after 12 years: accomplishments, remaining challenges, and potential impacts of COSMIC-2. *Bulletin of the American Meteorological Society*, *101*(7), E1107–E1136. doi: 10.1175/BAMS-D-18-0290.1

Hoffman, R., & Atlas, R. (2016). Future observing system simulation experiments. *Bull. of the Amer. Met. Soc.*, *97*, 1601–1616. doi: 10.1175/BAMS-D-15-00200.1

Holdaway, D., Errico, R., Gelaro, R., & Kim, J. (2014). Inclusion of linearized moist physics in NASA's Goddard Earth Observing System data assimilation tools. *Mon. Wea. Rev.*, *142*, 414–433. doi: 10.1175/MWR-D-13-00193.1

Kirk-Davidoff, R., Goody, M., & Anderson, J. (2005). Analysis of sampling errors for climate monitoring satellites. *J.Climate*, *19*, 810–823. doi: 10.1175/JCLI-3301.1

Leroy, S. (2001). The effects of orbital precession on remote climate monitoring. *J. Climate*, *14*, 4330–4337. doi: 10.1175/1520-0442(2001)014$⟨$4330:TEOOPO$⟩$2.0.CO;2

Li, L., Žagar, N., Raeder, K., & Anderson, J. (2023). Comparison of temperature and wind observations in the tropics in a perfect-model, global EnKF data assimilation system. *Quart. J. Roy. Meteor. Soc.*, *149*, 2367–2385. doi: 10.1002/qj.4511

Lorenz, E. N. (1969). The predictability of a flow which possesses many scales of motion. *Tellus*, *21*, 289–307. doi: 10.1111/j.2153-3490.1969.tb00444.x

McCarty, W., Carvalho, D., Moradi, I., & Prive, N. C. (2021). Observing system simulation experiments investigating atmospheric motion vectors and radiances from a constellation of 4-5 micro-m infrared sounders. *J. Atmos. Ocean Tech.*, *38*, 331–347. doi: 10.1175/JTECH-D-20-0109.1

McGrath-Spangler, E., McCarty, W., Privé, N., Moradi, I., Karpowicz, B., & McCorkel, J. (2022). Using OSSEs to evaluate the impacts of geostationary infrared sounders. *J. Atmos. Ocean Tech.*, *39*, 1903–1918. doi: 10.1175/JTECH-D-22-0033.1

Morel, P., & Talagrand, O. (1974). Dynamic approach to meteorological data assimilation. *Tellus-A*, *26*, 334–344. doi: 10.3402/tellusa.v26i3.9839

NOAA SPRWG. (2018). *NOAA Space Platform Requirements Working Group (SPRWG) Final (Cycle 2b) Report* (Tech. Rep.). NOAA/NESDIS. (https://repository.library.noaa.gov/view/noaa/48488)

Privé, N. C., Errico, R. M., & Akkraoui, A. E. (2022). Investigation of the potential saturation of information from global navigation satellite system radio occultation observations with an observing system simulation experiment. *Mon. Wea.*

Rev., *150*, 1293–1316. doi: 10.1175/mwr-d-20-0256.1
Privé, N. C., McGrath-Spangler, E., Carvalho, D., Karpowicz, B., & Moradi, I. (2023). Robustness of Observing System Simulation Experiments. *Tellus-A*, *75*, 309–333. doi: 10.16993/tellusa.3254
Privé, N. C., McGrath-Spangler, E., Karpowicz, B., & Kalluri, S. (2024). Impacts of an early morning low earth orbit observing platform in a future global observing network scenario. *Tellus-A*, *76*, 227–249. doi: 10.16993/tellusa.4080
Privé, N. C., McLinden, M., Lin, B., Heymsfield, G., Cai, X., & Harrah, S. (2024). Observing system simulation experiments exploring potential spaceborne deployment options for a differential absorption radar measuring marine surface pressures. *Earth and Space Science*, *11*. doi: 10.1029/2024ea003791
Rennie, M. (2010). The impact of GPS radio occultation assimilation at the Met Office. *Quart. J. Roy. Meteor. Soc.*, *102*, 116–131. doi: 10.1002/qj.521
Rienecker, M., Suarez, M., Todling, R., Bacmeister, J., Takacs, L., Liu, H.-C., ... Nielsen, J. (2008). *The GEOS-5 data assimilation system - documentation of versions 5.0.1, 5.1.0 and 5.2.0* (Tech. Rep. No. 27). NASA.
ROM SAF, E. (2021). The Radio Occultation Processing Package (ROPP) Forward Model Module User Guide Version 11. *SAF/ROM/METO/UG/ROPP/006*.
Ruston, B., & Healy, S. (2021). Forecast impact of FORMOSAT-7/COSMIC-2 GNSS radio occultation measurements. *Atmospheric Science Letters*, *22*(3). doi: 10.1002/asl.1019
Schreiner, W. S., Weiss, J., Anthes, R. A., Braun, J., Chu, V., Fong, J., ... others (2020). Cosmic-2 radio occultation constellation: First results. *Geophysical Research Letters*, *47*(4), e2019GL086841. doi: 10.1029/2019GL086841
Shao, H., Foelsche, U., Mannucci, A., Azeem, I., Bowler, N., Braun, J., ... Vergados, P. (2025). Advances in GNSS-based remote sensing for weather, climate, and space weather: Missions, applications, and emerging techniques. *Bull. of the Amer. Met. Soc.*. doi: 10.1175/BAMS-D-25-0138.1
Smagorinsky, J., Miyakoda, K., & Strickler, R. (1970). The relative importance of variables in initial conditions for dynamical weather prediction. *Tellus-A*, *22*, 141-157. doi: 10.1111/j.2153-3490.1970.tb01516.x
Vallis, G. (1991). Mechanisms and parameterizations of geostrophic adjustment and a variational approach to balanced flow. *J. Atmos. Sci.*, *49*, 1144–1160. doi: 10.1175/1520-0469(1992)049⟨1144:MAPOGA⟩2.0.CO;2
von Engeln, A., Healy, S., Marquardt, C., Andres, Y., & Sancho, F. (2009). Validation of operational GRAS radio occultation data. *Geophysical research letters*, *36*(17). doi: 10.1029/2009GL039968